

BAPS: A Fine-Grained Low-Precision Scheme for Softmax in Attention via Block-Aware Precision reScaling

Zisheng Ye ^{*1} Xiaoyu He ^{*1} Maoyuan Song¹ Guoliang Qiu¹ Chao Liao¹ Chen Wu¹ Yonggang Sun²
 Zhichun Li² Xiaoru Xie² Yuanyong Luo² Hu Liu² Pinyan Lu^{1,3} Heng Liao²

Abstract

As the performance gains from accelerating quantized matrix multiplication plateau, the softmax operation becomes the critical bottleneck in Transformer inference. This bottleneck stems from two hardware limitations: (1) limited data bandwidth between matrix and vector compute cores, and (2) the significant area cost of high-precision (FP32/16) exponentiation units (EXP2). To address these issues, we introduce a novel low-precision workflow that employs a specific 8-bit floating-point format (HiF8) and block-aware precision rescaling for softmax. Crucially, our algorithmic innovations make low-precision softmax feasible without the significant model accuracy loss that hampers direct low-precision approaches. Specifically, our design (i) halves the required data movement bandwidth by enabling matrix multiplication outputs constrained to 8-bit, and (ii) substantially reduces the EXP2 unit area by computing exponentiations in low (8-bit) precision. Extensive evaluation on language models and multi-modal models confirms the validity of our method. By alleviating the vector computation bottleneck, our work paves the way for doubling end-to-end inference throughput without increasing chip area, and offers a concrete co-design path for future low-precision hardware and software.

1. Introduction

Modern accelerators typically comprise two types of components. The first consists of general-purpose accelerators

^{*}Equal contribution ¹Taylor Lab, Huawei ²HiSilicon, Huawei ³Key Laboratory of Interdisciplinary Research of Computation and Economics, Shanghai University of Finance and Economics, Shanghai, China. Correspondence to: Pinyan Lu <lu.pinyan@mail.shufe.edu.cn>, Heng Liao <liao.heng@hisilicon.com>.

Preprint. February 3, 2026.

such as streaming multi-processors on GPU and Vector Cores on NPU (Liao et al., 2019), which contain a lot of arithmetic logic units (ALUs). The second type includes special-purpose accelerators, designed with domain-specific architectures (DSAs) to efficiently execute a small range of highly-demanded tasks. Since general matrix multiplications (GEMMs) are fundamental to a variety of diverse fields—including machine learning (Bishop, 2006), computer vision (Torralba et al., 2024), robotics (Murray et al., 1994), and scientific computing (Dongarra et al., 1998), such operations are commonly assigned onto special-purpose components for best performance. On NPUs, these are known as Cube Cores, while GPUs often employ Tensor Cores for such operations.

The advent of Transformer (Vaswani et al., 2017) has driven remarkable progress across artificial intelligence generated content (AIGC), powering breakthroughs in natural language processing and reasoning (OpenAI, 2024; Hu et al., 2024), video generation (Peebles & Xie, 2023), agent workflows (Wang et al., 2024a), and robotic controls (Sanghai & Brown, 2024). The most computationally intensive component in Transformer is the multi-head attention mechanism, which takes GEMMs and softmax normalizations as its technical cornerstone. To alleviate GEMMs bottlenecks, quantization (Hubara et al., 2018) has become a fundamental technique, reducing memory bandwidth and enabling efficient computation on dedicated hardware such as Nvidia Tensor Cores and Huawei Cube Cores. An alternative approach, BLASST (Yuan et al., 2025), has recently been proposed as a skip scheme to avoid the expensive computational cost paid on softmax computation. Attempts at integrating these two approaches have however been met with the hurdle of precision conversion: BLASST is a fundamentally independent technique from quantized GEMMs, that starts by converting the low-precision outputs from the previous stage back to high-precision at an additional overhead, and does not take full advantage of the reduced computation cost that quantization and reduced precision allows. Despite these observations, very few efforts have ever been placed on directly reducing the cost of softmax computation via low-precision arithmetic.

This paper introduces a novel low-precision workflow to address the softmax bottleneck in Transformer inference. By re-engineering the Flash-Attention (Dao, 2024) computation path, our method achieves two synergistic optimizations: (i) executing core softmax operations in low (8-bit) precision, and (ii) drastically cutting 50% of the data movement bandwidth between general and special-purpose compute units via mixed-precision techniques. Our workflow is compatible with existing quantized GEMM backends and complementary to softmax-skipping approaches like BLASST (Yuan et al., 2025). Crucially, we maintain model accuracy via a key algorithmic innovation—block-aware precision rescaling—thereby overcoming the substantial accuracy degradation typical of direct low-precision attempts.

Our design adopts a default low-precision (FP8) path for forwarding GEMMs results. A safeguard mechanism conditionally triggers high-precision rescaling based on a dynamic error analysis. This analysis monitors the discrepancy between a block’s local maximum and the global maximum propagated from previous blocks, dynamically signaling the need for increased precision. Empirically, rescaling and re-calculation are required in only 5% of cases in NLP and 10% of cases in multi-modal tasks, preserving the bulk of the FP8 efficiency gains. This approach implements a signal-guided, dynamic precision adaptation strategy, which seamlessly toggles precision levels to optimize the accuracy-efficiency trade-off.

1.1. Organization and overview

The rest of this paper is organized as follows. Section 2 surveys prior art on accelerating attention. Section 3 elaborates our proposed methodology. Section 4 evaluates our approach on diverse AIGC tasks, such as language and text-to-video generation. Section 5 concludes the paper.

2. Related Work

Low Precision and Sparse Attention A dominant trend in efficient transformer deployment is the aggressive quantization of linear operations, which reduces the bit-width of weights and activations to reduce memory bandwidth consumption and decrease the computational cost of GEMMs. The recent advancement in 4-bit training and inference (NVIDIA, 2025) is one of the typical examples of this trend. However, a critical challenge emerges within the attention block: while the linear operations can be computed efficiently in low precision, standard softmax modules force related arithmetic to be carried out in high precision, causing a “precision disparity”. Consequently, the attention pipeline is forced to switch between low-precision GEMMs for linear operations and high-precision floating-point operations within softmax module (Zhang et al., 2025), which costs computational resources spent on converting data between

different precisions and wastes the extra numerical accuracy obtained by high-precision arithmetic.

The adoption of mixed-precision systems has been bottlenecked by precision disparity discussed above. The huge gap of computing power difference between the 4-bit GEMMs on specific-purpose accelerators and 32-bit operations on general-purpose accelerators, which is more than 2 orders of magnitudes difference in terms of floating operations per second (Flops) on the most advanced systems (Nvidia, 2025), results in low utilization rate of specific-purpose accelerators. The utilization rate is only around 30% (Zhang et al., 2025) on consumer-level devices, and expected to be even lower on more advanced systems. Although recently proposed sparse schemes, e.g., BLASST (Yuan et al., 2025), can skip 50% of the computation in attention modules without loss in accuracy. Yet, for the remaining, unavoidable computations that must be executed, the high-precision softmax operation continues to create a disparity with the low-precision GEMMs. This persistent precision mismatch leaves the hardware utilization bottleneck largely unaddressed, underscoring the need for fundamental low-precision softmax designs.

Co-designed Approximations for Softmax On top of algorithmic innovations like Flash-Attention (Dao, 2024) that aim to reduce the memory footprint of attention mechanisms, another parallel line of research focuses on the softmax operation itself. These works employ hardware-software co-design to accelerate or approximate the expensive exponentiation and normalization steps inherent to the softmax operation.

One prominent strategy, exemplified by Stevens et al. (Stevens et al., 2021), seeks to approximate the softmax operation to reduce its hardware cost. Their work, “Soft-ermax”, proposes replacing high-precision floating-point exponentiation with a low-cost, piecewise first-order approximation of the $\exp 2$ function using integer arithmetic. While this approach achieves notable gains in area and energy efficiency, it also introduces fundamental limitations that likely hindered its widespread adoption: the first-order approximation can incur non-negligible numerical errors, which poses a potential risk for tasks involving long sequences or requiring high numerical fidelity because the error can accumulate across iterations. Furthermore, the proposed design focuses on the computation itself but does not optimize the memory bandwidth at the *input* of the softmax module. The preceding attention scores are typically still calculated and transferred in high precision, meaning the memory bandwidth preceding the softmax module remains a performance and energy constraint, limiting the end-to-end benefit.

The attention module has multiple computation operations

that can be fused together to minimize intermediate data read and write operations and enable low-precision approximations to reduce the intermediate memory access expense. Alexandridis et al. (Alexandridis et al., 2025) propose a solution that fuses exponentiation and multiplication into a single hardware unit which adopts shift operations to save the computation delay and avoids the computation of exponents in high precision and uses shift operations to save the computation delay. Similarly, Wang et al. (Wang et al., 2025) take a broader co-design view, not only fusing internal softmax steps but also combining softmax and the layer normalization operations into a unified hardware pipeline. This fuses two consecutive stages in attention and greatly reduces the control and data transfer overhead across multiple layers. Although these fusion-based methods align with the memory-bound nature of attention, their shared major drawback is increased hardware specialization and inflexibility for supporting emerging algorithmic variants or alternative normalization schemes.

Low Precision Data Formats Several data formats exist for low-precision floating numbers. For 16-bit representations, FP16 and BF16 are the most common ones. BF16 retains the same number of exponent bits as FP32, resulting in a larger dynamic range compared to FP16. This makes BF16 more robust against outliers and better at capturing gradients during training. Thus, BF16 is preferred for training neural networks. When it comes to 8-bit floating numbers, a wider variety of formats are available. Single numbers can typically be represented using E4M3 (4 exponent bits and 3 mantissa bits) or E5M2 (5 exponent bits and 2 mantissa bits). To balance memory footprint with numerical accuracy, MXFP8 (Mishra et al., 2025) has been recently introduced for training LLMs. In MXFP8, multiple numbers share a common scaling factor while each is stored in E4M3 format. After scaling, MXFP8 can achieve a dynamic range comparable to that of E5M2 but with higher accuracy. MXFP8 is especially suitable for linear operations such as matrix multiplications, where scaling factors and data can be efficiently separated. An alternative approach to extend the dynamic range of data is to consider the recently introduced 8-bit format - HiF8 (Luo et al., 2024). HiF8 employs a dynamic exponent-mantissa coding scheme that simultaneously expands the representable range and maintains accuracy. Unlike MXFP8, it does not rely on shared scaling factors, making it a suitable choice for complex nonlinear computations.

3. Approach

Consider query $\mathbf{Q} = [\mathbf{Q}_0; \mathbf{Q}_1; \dots; \mathbf{Q}_{N_Q}] \in \mathbb{R}^{s_q \times d}$, key $\mathbf{K} = [\mathbf{K}_0; \mathbf{K}_1; \dots; \mathbf{K}_{N_K}] \in \mathbb{R}^{s_k \times d}$ and value $\mathbf{V} = [\mathbf{V}_0; \mathbf{V}_1; \dots; \mathbf{V}_{N_K}] \in \mathbb{R}^{s_k \times d}$, where s_q and s_k is the sequence length of query and key, and d is the head dimension.

The standard attention is computed as follows:

$$\mathbf{O} = \mathbf{P}\mathbf{V} = \text{softmax}(\mathbf{S})\mathbf{V} = \text{softmax}\left(\frac{\mathbf{Q}\mathbf{K}^\top}{\sqrt{d}}\right)\mathbf{V}, \quad (1)$$

where $\mathbf{S} = (\mathbf{Q}\mathbf{K}^\top)/\sqrt{d}$ is the scaled dot-product scores. The core component of this computation is the nonlinear softmax function (Bishop, 2006), which normalizes the scaled dot-product scores to produce a valid probability distribution over keys for each query.

As s_q and s_k can be very large in the general purpose tasks, Flash Attention (FA) (Shah et al., 2024; Dao, 2024) is employed to accelerate computation and avoids storing large-sized intermediate results, most notably the attention score matrix $\mathbf{S} \in \mathbb{R}^{s_q \times s_k}$. The core iterative step of FA can be expressed as follows:

$$\begin{aligned} \mathbf{S}_i^{(j)} &= \mathbf{Q}_i \mathbf{K}_j^\top \cdot \frac{\log_2 e}{\sqrt{d}} \\ \mathbf{m}_i^{(j)} &= \text{rowmax}([\mathbf{m}_i^{(j-1)}, \text{rowmax}(\mathbf{S}_i^{(j)})]) \\ \mathbf{P}_i^{(j)} &= 2^{\mathbf{S}_i^{(j)} - \text{rowfill}(\mathbf{m}_i^{(j)})} \\ \mathbf{d}_i^{(j)} &= \text{diag}(2^{\mathbf{m}_i^{(j-1)} - \mathbf{m}_i^{(j)}}) \mathbf{d}_i^{(j-1)} + \mathbf{P}_i^{(j)} \mathbf{1} \\ \tilde{\mathbf{O}}_i^{(j)} &= \text{diag}(2^{\mathbf{m}_i^{(j-1)} - \mathbf{m}_i^{(j)}}) \tilde{\mathbf{O}}_i^{(j-1)} + \mathbf{P}_i^{(j)} \mathbf{V}_j, \end{aligned} \quad (2)$$

in which $\mathbf{S}_i^{(j)}$ denotes the scaled dot-product scores between the i -th query tile and the j -th key tile, $\mathbf{m}_i^{(j)}$ denotes the vector storing the row-wise maximum values used for numerical stabilization, $\mathbf{d}_i^{(j)}$ represents the denominator vector in the online softmax computation, and $\tilde{\mathbf{O}}_i^{(j)}$ denotes the corresponding un-normalized attention output. Moreover, $\text{rowfill}(\cdot)$ expands a vector into a matrix by replicating each element of the input vector across an entire row, such that every row of the resulting matrix is a constant vector equal to the corresponding element of the input. Conversely, $\text{rowsum}(\cdot)$ reduces a matrix to a vector by summing the elements along each row.

In most of the open-source models (Team Wan, 2025), the query, key and value matrices (\mathbf{Q} , \mathbf{K} , \mathbf{V}) are typically stored as BF16 format. To reduce the memory bandwidth requirements and computational resources, post-training quantization (PTQ) (Frantar et al., 2022) or activation-aware weight quantization (AWQ) (Lin et al., 2023) can be applied, typically with negligible degradation in model accuracy. Micro-scaling (e.g., Zhang et al., 2025) can alternatively reduce the cost of attention computation as well. Consequently, while existing methods successfully reduce the precision of \mathbf{Q} , \mathbf{K} , and \mathbf{V} to as low as FP8 or even FP4, the precision of \mathbf{S} and the subsequent softmax normalization \mathbf{P} remain constrained to be as high as BF16/FP16 or even FP32. This leaves the precision disparity within the attention block unresolved.

Meanwhile, modern accelerators mitigate the workload of

matrix-matrix products by employing special-purpose accelerators, e.g., Tensor cores on Nvidia GPUs. It splits the procedure into multiple individual stages running on special-purpose and general-purpose accelerators separately. This results in potentially varying precision requirements between different stages. In the case of Flash Attention (2), although the accumulator produces outputs in 32-bit precision, maintaining the same precision throughout the softmax calculation is unnecessary. By leveraging quantization techniques, the matrix product \mathbf{PV} in Equation (1) can even take 4-bit numbers as the inputs without much loss. This suggests that performing all softmax operations in 32-bit precision introduces significant redundancy.

Motivated by this observation, we investigate efficient attention computation using reduced numerical precision, which can substantially save resources while preserving end-to-end model accuracy. This section details our strategies to reduce the cost of computing attention in Equation (1). Our key insight is that the matrix \mathbf{P} inherently tolerates low precision. Consequently, we first propose computing \mathbf{P} directly in 8-bit precision for the exponential operations without quantization steps (Section 3.1). To further reduce memory traffic bottleneck when shuttling data between special-purpose and general-purpose accelerators, we propose storing the attention scores \mathbf{S} in 8-bit format (Section 3.2). To combat the multiplication error accumulation in online softmax, we further propose to compute exponentials using base-2 raised to integer exponents. This approach significantly improves numerical accuracy while maintaining low-precision efficiency (Section 3.3). All these methods are integrated and simplified using the HiF8 format (Luo et al., 2024), with the complete workflow summarized in Section 3.4.

3.1. 8-bit Exponents (P)

As noted above, the exponentiation operation does not require high precision. For example, in most accelerated inference scenarios (Zhang et al., 2025), the exponentiated result \mathbf{P} can be cast to lower precision before the matrix multiplication with \mathbf{V} . Since $\mathbf{S}_i^{(j)} - \text{rowfill}(\mathbf{m}_i^{(j)})$ is predominantly negative and confined to a moderate numerical range (given appropriate head dimension and normalization scaling), we represent it using an 8-bit low-precision format prior to exponentiation.

There are two typical FP8 formats-E4M3 and E5M2, where E4M3 is strongly preferred for representing $\mathbf{S}_i^{(j)} - \text{rowfill}(\mathbf{m}_i^{(j)})$ due to its larger mantissa. This yields a quantized distribution that more closely approximates the original FP32 values, as shown in Figure 1a. Conversely, exponentiating two by this difference compresses the range of $\mathbf{P}_i^{(j)}$ within $[0, 1]$ (see Figure 1b), presenting a distinct challenge: for values in $[0, 2^{-9}]$, E4M3 lacks sufficient resolution, which limits the model’s expressive capacity. E5M2,

with its larger dynamic range, is therefore better suited for representing \mathbf{P} .

These observations motivates a “mixed format” strategy, rather than using only E4M3 or E5M2 exclusively. As shown in Figure 1a, the distributions of the powers-of-two operation results under different input/output precision formats are compared against the FP32 baseline.

The orange and green curves represent pure E4M3 and pure E5M2 configurations, respectively, while the red curve corresponds to the mixed-format approach (E4M3 input, E5M2 output). This hybrid scheme most closely approximates the FP32 reference distribution. However, it introduces added complexity in both software and hardware implementation. Consequently, as discussed in Section 3.4, we adopt HiF8 (Luo et al., 2024) as a more practical and efficient alternative.

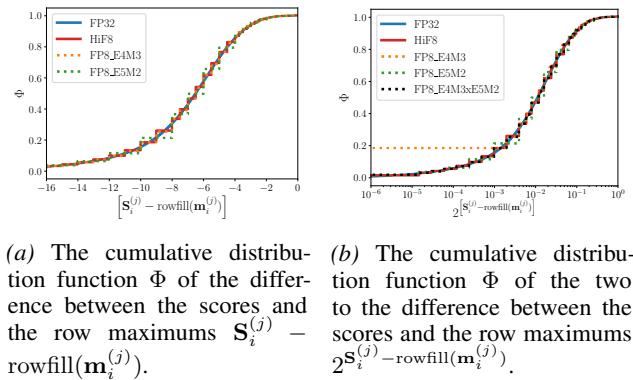


Figure 1. The cumulative distribution function Φ of different data formats. The scores are dumped from Qwen3-30B-A3B-Instruct model.

3.2. Towards 8-bit Attention Scores (S)

Our computational reorganization is motivated by a hardware-aware precision trade-off: although the score matrix $\mathbf{S}_i^{(j)}$ itself lacks sufficient precision in 8-bit representation, the difference form $\mathbf{S}_i^{(j)} - \text{rowfill}(\mathbf{m}_i^{(j)})$ can be cast to 8-bit with acceptable accuracy. In the standard Flash Attention pipeline, however, this subtraction occurs on the general-purpose accelerators (e.g., Vector/Cuda Cores) after $\mathbf{S}_i^{(j)}$ is transferred from the special-purpose accelerators (e.g., Cube/Tensor Cores). Therefore, simply casting the subtraction result to 8-bit post-computation does not reduce the dominant memory traffic of $\mathbf{S}_i^{(j)}$. To capture this benefit, the low-precision computation casting must be moved earlier in the pipeline.

We therefore propose to offload the critical subtraction step. Instead of transferring the full-precision $\mathbf{S}_i^{(j)}$ as in Equa-

tion (2), we let special-purpose accelerators compute:

$$\mathbf{T}_i^{(j)} = \mathbf{S}_i^{(j)} - \text{rowfill}(\tilde{\mathbf{m}}_i^{(j)}) , \quad (3)$$

where $\tilde{\mathbf{m}}_i^{(j)}$ is an “approximate” row-wise maximum, initialized as $\tilde{\mathbf{m}}_i^{(j)} = \mathbf{m}_i^{(j-1)}$ (i.e., the maximum from the previous iteration). $\mathbf{T}_i^{(j)}$ is then transferred to general-purpose accelerators in 8-bit low precision form. An update of $\tilde{\mathbf{m}}_i^{(j)}$ and a recalculation of $\mathbf{T}_i^{(j)}$ could be triggered conditionally, based on the value range of $\mathbf{T}_i^{(j)}$ and controlled by a restart threshold λ .

Once the “approximate” row-wise maximums $\tilde{\mathbf{m}}_i^{(j)}$ are obtained, they are transferred to the special-purpose accelerators. The subtraction is then performed before the result is sent to the general-purpose accelerators, effectively operating on lower-precision data earlier. This approximation is effective due to the systematic bias in the distribution of row-wise maxima in attention scores (Kaul et al., 2024), where certain tiles are significantly more likely to contain the global maximum. For example, in auto-regressive language modeling, the first and last tiles often exhibit this property.

We denote the set of such critical tiles as \mathcal{B}_0 , and the remaining tiles as \mathcal{B}_1 . For tiles in \mathcal{B}_0 , which are evaluated first, $\mathbf{m}_i^{(j)}$ is already a close approximation to the final global maximum. Consequently, for a majority of subsequent tiles, $\mathbf{T}_i^{(j)}$ (calculated using the approximate maximum) is accurate enough for downstream computations, and preserving $\mathbf{T}_i^{(j)}$ in high precision yields diminishing returns.

3.3. Reduce Accumulated Error of Power-of-2 Computations

Following (Stevens et al., 2021), we restrict the use of powers of two to integer exponents, specifically for the rescaling factor when updating $\mathbf{d}_i^{(j)}$ and $\tilde{\mathbf{O}}_i^{(j)}$. Because these updates recur as the sequence length scales, low-precision operations can cause numerical errors to accumulate over iterations. Figure 2 illustrates how this error propagates with increasing sequence length. To mitigate the accumulated multiplicative error, we propose using integer powers of two. Crucially, unlike general exponentiation or powers of two with arbitrary (non-integer) exponents, integer powers of two are exact and introduce no additional numerical error. Consequently, as evidenced in Figure 2, the error remains tightly bounded when integer powers of two are used for cumulative updates. This approach necessitates rounding each entry in $\mathbf{S}_i^{(j)}$ to update $\mathbf{m}_i^{(j)}$ in Equation (2). The complete reorganized attention formulation is presented in Algorithm 1.

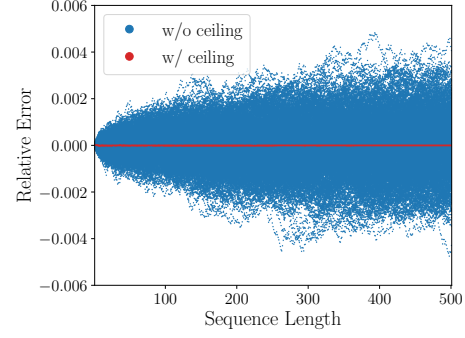


Figure 2. Illustration of numerical error in accumulative products: a comparison between exponents of 2 with integers and direct exponents of 2 against FP32 ground truth.

3.4. Summary of the Proposed Method

The complete workflow is summarized in Algorithm 1. Our method modifies the standard Flash Attention (Equation (2)) by integrating the subtraction of the row maximum from the scores directly into the computation of the $\mathbf{Q}_i \mathbf{K}_j^\top$ products.

This can be fused with the dequantization step when \mathbf{Q}_i and \mathbf{K}_j are hardware-quantized. The row max $\mathbf{m}_i^{(j)}$ is always rounded to the nearest integer for enhancing the numerical accuracy when updating $\mathbf{d}_i^{(j)}$ and $\tilde{\mathbf{O}}_i^{(j)}$. Furthermore, leveraging the prior pattern of the row-wise maximum discussed in Section 3.2, the value of $\mathbf{m}_i^{(j)}$ can often be predicted with high confidence by examining a small subset of tiles in advance. This allows the update for $\mathbf{m}_i^{(j)}$ to be skipped in the majority of tile iterations, improving efficiency. For hardware optimization, the powers of 2 in the calculation of $\mathbf{P}_i^{(j)}$ are computed using the HiF8 format, which reduce circuit area and increases throughput for this nonlinear operation.

To control the accuracy of the attention outputs, the accuracy of approximate row-wise maximum $\tilde{\mathbf{m}}_i^{(j)}$ can be adjusted dynamically based on the value of $\text{rowmax}(\mathbf{T}_i^{(j)})$. Specifically, if the maximum entry in $\text{rowmax}(\mathbf{T}_i^{(j)})$ exceeds a predefined threshold λ , the scores are recalculated and stored in high precision for subsequent processing on general-purpose accelerators. The numerical results in Table 4 indicate that such rescaling and recalculation events are very rare, as $\text{rowmax}(\mathbf{T}_i^{(j)})$ is typically non-positive. Consequently, with high probability, the recalculation of $\mathbf{T}_i^{(j)}$, as well as the rescaling of $\mathbf{d}_i^{(j-1)}$ and $\tilde{\mathbf{O}}_i^{(j-1)}$ can be avoided.

4. Ablation Experiments

In this section, we examine the proposed workflow for both language model and multi-modal model.

4.1. Experimental Setups

We evaluate our proposed method under three configurations:

- **Default:** In this configuration, We compute the $\text{softmax}(\cdot)$ as stated in Equation (2) with inputs stored in BF16 and all operations within the softmax performed in FP32.

- **Exp2 HiF8:** This configuration is identical to the **Default** configuration, except that all power-of-two exponentiation operations in the softmax use the HiF8 data format. This targets the most computationally expensive operation in the softmax by employing HiF8 arithmetic.

- **E2E HiF8:** This configuration computes the softmax as defined in Algorithm 1, with inputs stored in BF16 and HiF8 extended to nearly all operations within the softmax module. The first tile in each input sequence is assigned to \mathcal{B}_0 , and the remaining tiles to \mathcal{B}_1 , as specified in Algorithm 1. Unless otherwise specified, we set $\lambda = 1$.

All experiments use the same random seed to ensure consistent randomness across configurations, guaranteeing a fair ablation study.

4.2. The Language Models' Accuracy

Since large-scale models are more robust to numerical errors from low-precision arithmetic, small-scale models offer a more challenging and effective test for validating our proposed method. To evaluate the sensitivity of low-precision operations in natural language processing, we focus on small-scale models containing fewer than 50B parameters—approximately one-tenth the size of flagship open-source models such as DeepSeek-V3(DeepSeek-AI, 2025). We primally focus on Qwen3-30B-A3B-Instruct-2507 (Team, 2025) and also adopt the smaller Llama-3.1-8B (Team, 2024) as the language models in various benchmarks.

In order to verify the advantage of HiF8 over other FP8 formats, we first use the common word extraction task (CWE) in RULER (Hsieh et al., 2024), the empirically sensitive sub-task in RULER when varying the input sequence lengths, for the comparison. We consider three different sequence lengths of input tokens, 32K, 64K and 96K, in the task. For each sequence length, the test dataset is composed by 100 randomly generated samples. Three additional setups are considered by following the setup of **Exp2 HiF8** except with different input/output data formats for exponentiation:

- 1) **Exp2 E4M3:** using E4M3 for both input/output,

- 2) **Exp2 E5M2:** using E5M2 for both input/output,
- 3) **Exp2 E4M3xE5M2:** using E4M3 for input and E5M2 for output,
- 4) **Naive E2E:** directly converting scores to HiF8 before subtraction with row maximum.

As shown in Table 1, the **Exp2 E4M3** format incurs substantial accuracy loss on the CWE task, aligning with the power distribution analysis in Figure 1b and the discussion in Section 3.1. A detailed comparison at sequence length 64K (where the **Default** baseline exceeds 60% accuracy) reveals that **Exp2 E4M3xE5M2** and our proposed **Exp2 HiF8** consistently outperform other FP8 configurations. This validates the advantage of the HiF8 format for low-precision softmax exponentiation, a design choice justified by its adaptive range and implementation simplicity. Converting to FP8 after subtraction and the restart mechanism is essential to the success of **E2E HiF8** setup for ensuring the models’ accuracy when comparing the results from **Naive E2E** which directly converting scores to HiF8 without modifying the original workflow of Flash-Attention.

The evaluation of the proposed method on language reasoning is conducted on the MMLU-Pro benchmark suite (Wang et al., 2024b), GPQA-Diamond (Rein et al., 2023), and MATH-500 dataset (Lightman et al., 2023). The results are reported in Table 2, only using a single shot for each test sample.

Comparing to **Default** setup, both **Exp2 HiF8** and **E2E HiF8** show a comparable overall accuracy with at most 1% degradation in the quantitative results across different models and different benchmark suites, except GPQA-Diamond on Llama-3.1. This is a highly promising result, as adopting HiF8 can significantly reduce exponentiation operations consumption and thereby improve the computational throughput of the softmax module. Moreover, **E2E HiF8** offers even greater throughput gains by at least halving the memory bandwidth required when transferring data from special-purpose accelerators to general-purpose ones.

However, certain sub-tasks exhibits notable accuracy fluctuation which are all highlighted in red in Table 5-8. This suggests that different tasks vary considerably in their sensitivity to numerical precision. To mitigate this issue and ensure robust performance across diverse downstream tasks, post-processing, e.g., PTQ, is required to make the model aware of low-precision arithmetic and improve the accuracy for different kinds of downstream tasks before deploying the proposed inference acceleration scheme.

4.3. The Multi-modal Models’ Accuracy

We adopt the multi-modal model Wan-2.2 (Team Wan, 2025) as our testbed to evaluate the proposed method on the text-

Setup \ Seq Len	32K	64K	96K
Default	88.5	64.8	58.9
Exp2 E4M3	86.1	58.1	53.0
Exp2 E5M2	87.8	62.4	58.5
Exp2 E4M3xE5M2	87.5	63.5	57.4
Exp2 HiF8	89.1	63.2	58.1
E2E HiF8	88.0	64.0	58.3
Naive E2E	87.8	54.0	44.0

Table 1. Accuracy of Qwen3-30B-A3B on CWE with various input lengths of tokens. The accuracy is calculated in percentage and higher values are preferable.

Model	Benchmark	Default	Exp2 HiF8	E2E HiF8
Qwen3	MMLU-P	73.59	72.96	72.53
	GPQA-D	54.55	57.58	58.59
	MATH500	78.40	80.00	79.80
Llama-3.1	MMLU-P	46.01	45.51	45.19
	GPQA-D	30.81	25.76	28.79
	MATH500	46.80	46.40	47.60

Table 2. Accuracy on different tasks in NLP With different setups. The accuracy is calculated in percentage and higher values are preferable.

to-video (T2V) generation task. Similar to the language models, the advantage of the proposed workflow can be easily verified with a simple experiment as shown in Figure 3. This experiment only generates a single frame with forty sampling steps. Only setup **Naive E2E** generated a blurred frame, while the other three setups all generated consistent results in high quality.

8 prompts for T2V task is considered. The generated frames are shown in Figure 5-Figure 12. To quantitatively analyze the quality of the generated videos, the average cosine similarity (Similarity), the average mean squared error (MSE), the average structural similarity index (SSIM), and the average peak signal-to-noise ratio (PSNR) across 8 generated videos are reported in Table 3. It compares the videos generated from setup **Exp2 HiF8** and **E2E HiF8** to **Default** setup, respectively. For both $\lambda = 1$ and $\lambda = 2$ shown in Table 3, it shows only 1% difference in the similarity between these two setups. This validates setup **E2E HiF8** is capable to be deployed for low-precision inference acceleration for harnessing extra savings on memory bandwidth consumption.

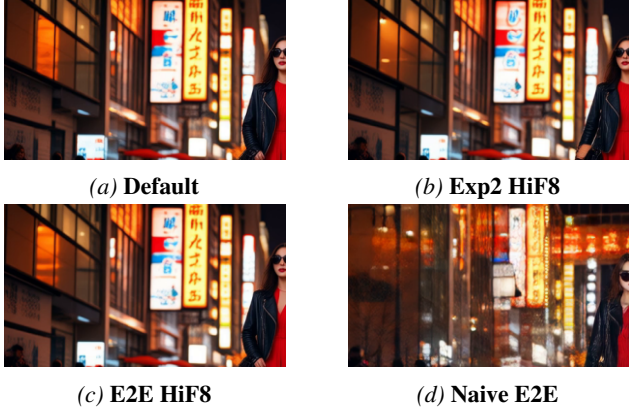


Figure 3. The single frame generated from different setups using Wan-2.2. The illustration only shows the upper-left sub-frame for each setup. Only setup **Naive E2E** generated blurred frame and the other three frames are consistent with each other in a high quality.

4.4. The Restart Rate

Other than the quantitative accuracy metrics, we also evaluate the cost associated with restart events. Each restart requires recalculation and transmission of scores in high precision, which breaks the Flash Attention pipeline and diminishes the time savings gained from low-precision exponentiation. To quantify the restart rate, we use the CWE-32K benchmark for NLP tasks and the first prompt from Appendix Figure 5 for the T2V task.

We count the number of restarted tiles in each run of Algorithm 1 and compute the Average Restart Rate (ARR) for the entire testbed. ARR reflects the average probability that a tile’s $S_i^{(j)}$ requires high-precision recalculation. We also record the Peak Restart Rate (PRR) from any single calculation of \mathbf{O}_i to estimate worst-case costs. The overall restart rates are presented in Table 4, and the probability density of restart rates per run is shown in Figure 4. Since the method updates $\mathbf{d}_i^{(j)}$ and $\tilde{\mathbf{O}}_i^{(j)}$ using integer powers of two to minimize accumulated error, the valid restart threshold λ is constrained to integers. Thus, we experiment with $\lambda = 0, 1, 2$ in the experiment.

Task Type	Metric	λ		
		0.0	1.0	2.0
NLP	ARR	10.86%	4.97%	2.50%
	PRR	96.67%	91.30%	87.50%
T2V	ARR	22.88%	10.48%	5.07%
	PRR	87.89%	67.19%	61.72%

Table 4. Restart rate analysis of different restart thresholds λ . ARR denotes the average restart rate of each tile and PRR denotes the peak restart rate of any single calculation of \mathbf{O}_i .

Metric	Exp2 HiF8	E2E HiF8	
		$\lambda = 1$	$\lambda = 2$
Similarity(\uparrow)	0.9561	0.9503	0.9485
MSE(\downarrow)	1678.3	1826.13	1910.67
SSIM(\uparrow)	0.6511	0.6347	0.6225
PSNR(\uparrow)	19.446	18.875	18.389

Table 3. Evaluation of Wan-2.2 on T2V tasks With different setups. Similarity, SSIM and PSNR are positively correlated with the generated contents’ quality. MSE is negatively correlated with the generated contents’ quality.

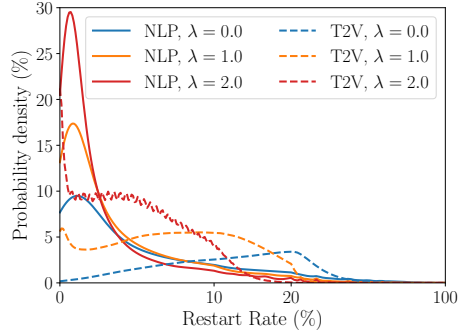


Figure 4. Probability density of restart rates for both NLP and T2V tasks. The solid line represents the density of NLP task and the dashed line represents the density of T2V task.

Compared with $\lambda = 0$, setting $\lambda = 1$ halves the ARR for both tasks. Given the negligible impact on model accuracy, **E2E HiF8** effectively harnesses the benefits of re-

duced memory bandwidth consumption, incurring only minor overhead from occasional high-precision recalculations. By tuning the restart threshold, it can also deliver a trade-off between models’ accuracy and throughput. This tunability provides flexibility, enabling the proposed scheme to be adapted to systems with varying requirements. Besides ARR, PRR is another key indicator for evaluating the overhead of **E2E HiF8** setup. Although increasing the restart threshold does not sharply reduce the PRR as shown in Table 4, Figure 4 suggests that such high-restart cases are rare and thus unlikely to impact end-to-end inference throughput in practice.

5. Conclusion

In conclusion, this paper tackles the softmax bottleneck in Transformer attention by proposing a novel low-precision workflow based on 8-bit computation and block-aware rescaling. Our scheme addresses two key hardware limitations: (1) it halves the data movement bandwidth by constraining matrix multiplication outputs to 8-bit, and (2) it drastically reduces the area cost of exponentiation units by computing exponents in low (8-bit) precision. Evaluated across both language and multi-modal models, our method validates a concrete hardware-software co-design path, effectively doubling inference throughput potential without additional chip area. The approach is readily applicable to NLP and AIGC tasks with minimal adaptations. Future work will explore the interaction of our scheme with quantized attention inputs and its integration with lossless sparse attention methods like BLASST (Yuan et al., 2025) for further gains. To maximize quality, integrating post-training techniques with our low-precision scheme is essential, as the model is agnostic to the arithmetic precision shift. Ultimately, extending this paradigm to the pre-training stage offers a promising avenue for reducing overall training costs.

References

Alexandridis, K., Titopoulos, V., and Dimitrakopoulos, G. Low-cost FlashAttention with fused exponential and multiplication hardware operators, 2025. URL <https://arxiv.org/abs/2505.14314>.

Bishop, C. M. *Pattern Recognition and Machine Learning*. Information Science and Statistics. Springer, 2006. ISBN 978-0387310732.

Dao, T. FlashAttention-2: Faster attention with better parallelism and work partitioning. In *The Twelfth International Conference on Learning Representations*, 2024. URL <https://openreview.net/forum?id=mZn2Xyh9Ec>.

DeepSeek-AI. DeepSeek-v3 technical report, 2025. URL <https://arxiv.org/abs/2412.19437>.

Dongarra, J. J., Duff, I. S., Sorensen, D. C., and van der Vorst, H. A. *Numerical Linear Algebra for High-Performance Computers*. Society for Industrial and Applied Mathematics, Philadelphia, PA, 1998. ISBN 0-89871-428-1.

Frantar, E., Ashkboos, S., Hoefer, T., and Alistarh, D. Gptq: Accurate post-training quantization for generative pre-trained transformers. *ArXiv*, abs/2210.17323, 2022. URL <https://api.semanticscholar.org/CorpusID:253237200>.

Hsieh, C.-P., Sun, S., Kriman, S., Acharya, S., Rekesh, D., Jia, F., Zhang, Y., and Ginsburg, B. RULER: What’s the real context size of your long-context language models? *arXiv preprint arXiv:2404.06654*, 2024.

Hu, Y., Tang, X., Yang, H., and Zhang, M. Case-based or rule-based: How do transformers do the math?, 2024. URL <https://arxiv.org/abs/2402.17709>.

Hubara, I., Courbariaux, M., Soudry, D., El-Yaniv, R., and Bengio, Y. Quantized neural networks: Training neural networks with low precision weights and activations. *Journal of Machine Learning Research*, 18(187):1–30, 2018. URL <http://jmlr.org/papers/v18/16-456.html>.

Kaul, P., Ma, C., Elezi, I., and Deng, J. From attention to activation: Unravelling the enigmas of large language models. *arXiv preprint arXiv:2410.17174*, 2024.

Liao, H., Tu, J., Xia, J., and Zhou, X. Davinci: A scalable architecture for neural network computing. In *2019 IEEE Hot Chips 31 Symposium (HCS)*, pp. 1–44, 2019. doi: 10.1109/HOTCHIPS.2019.8875654.

Lightman, H., Kosaraju, V., Burda, Y., Edwards, H., Baker, B., Lee, T., Leike, J., Schulman, J., Sutskever, I., and Cobbe, K. Let’s verify step by step, 2023. URL <https://arxiv.org/abs/2305.20050>.

Lin, J., Tang, J., Tang, H., Yang, S., Dang, X., and Han, S. Awq: Activation-aware weight quantization for LLM compression and acceleration. *ArXiv*, abs/2306.00978, 2023. URL <https://api.semanticscholar.org/CorpusID:271271084>.

Luo, Y., Zhang, Z., Wu, R., Liu, H., Jin, Y., Zheng, K., Wang, M., He, Z., Hu, G., Chen, L., Hu, T., Wang, J., Chen, M., Dmitry, M., Vladimir, K., Maxim, B., Hu, Y., Chen, G., and Huang, Z. Ascend hifloat8 format for deep learning, 2024. URL <https://arxiv.org/abs/2409.16626>.

Mishra, A., Stosic, D., Layton, S., and Micikevicius, P. Recipes for pre-training LLMs with MXFP8, 2025. URL <https://arxiv.org/abs/2506.08027>.

Murray, R. M., Li, Z., and Sastry, S. S. *A Mathematical Introduction to Robotic Manipulation*. CRC Press, Boca Raton, FL, 1994. ISBN 9780849379819.

NVIDIA. Pretraining large language models with NVFP4, 2025. URL <https://arxiv.org/abs/2509.25149>.

Nvidia. Nvidia blackwell architecture technical brief, 2025. URL <https://resources.nvidia.com/en-us-blackwell-architecture>.

OpenAI. GPT-4 technical report, 2024. URL <https://arxiv.org/abs/2303.08774>.

Peebles, W. and Xie, S. Scalable diffusion models with transformers, 2023. URL <https://arxiv.org/abs/2212.09748>.

Rein, D., Hou, B. L., Stickland, A. C., Petty, J., Pang, R. Y., Dirani, J., Michael, J., and Bowman, S. R. GPQA: A graduate-level Google-Proof Q&A benchmark, 2023. URL <https://arxiv.org/abs/2311.12022>.

Sanghai, N. and Brown, N. B. Advances in transformers for robotic applications: A review, 2024. URL <https://arxiv.org/abs/2412.10599>.

Shah, J., Bikshandi, G., Zhang, Y., Thakkar, V., Ramani, P., and Dao, T. FlashAttention-3: Fast and accurate attention with asynchrony and low-precision. In *The Thirty-eighth Annual Conference on Neural Information Processing Systems*, 2024. URL <https://openreview.net/forum?id=tVConYid20>.

Stevens, J. R., Venkatesan, R., Dai, S., Khailany, B., and Raghunathan, A. Softmax: Hardware/software co-design of an efficient softmax for transformers. In *2021 58th ACM/IEEE Design Automation Conference (DAC)*, pp. 469–474, 2021. doi: 10.1109/DAC18074.2021.9586134.

Team, L. The Llama 3 herd of models, 2024. URL <https://arxiv.org/abs/2407.21783>.

Team, Q. Qwen3 technical report, 2025. URL <https://arxiv.org/abs/2505.09388>.

Team Wan. Wan: Open and advanced large-scale video generative models, 2025. URL <https://arxiv.org/abs/2503.20314>.

Torralba, A., Isola, P., and Freeman, W. *Foundations of Computer Vision*. Adaptive Computation and Machine Learning series. MIT Press, 2024. ISBN 9780262378666. URL <https://mitpress.mit.edu/9780262048972-foundations-of-computer-vision/>.

Vaswani, A., Shazeer, N., Parmar, N., Uszkoreit, J., Jones, L., Gomez, A. N., Kaiser, L., and Polosukhin, I. Attention is all you need. *CoRR*, abs/1706.03762, 2017. URL <https://arxiv.org/abs/1706.03762>.

Wang, L., Ma, C., Feng, X., Zhang, Z., Yang, H., Zhang, J., Chen, Z., Tang, J., Chen, X., Lin, Y., Zhao, W. X., Wei, Z., and Wen, J. A survey on large language model based autonomous agents. *Frontiers of Computer Science*, 18(6), March 2024a. ISSN 2095-2236. doi: 10.1007/s11704-024-40231-1. URL <http://dx.doi.org/10.1007/s11704-024-40231-1>.

Wang, W., Zhou, S., Sun, W., Sun, P., and Liu, Y. Sole: Hardware-software co-design of softmax and layernorm for efficient transformer inference, 2025. URL <https://arxiv.org/abs/2510.17189>.

Wang, Y., Ma, X., Zhang, G., Ni, Y., Chandra, A., Guo, S., Ren, W., Arulraj, A., He, X., Jiang, Z., Li, T., Ku, M., Wang, K., Zhuang, A., Fan, R., Yue, X., and Chen, W. MMLU-Pro: A more robust and challenging multi-task language understanding benchmark, 2024b. URL <https://arxiv.org/abs/2406.01574>.

Yuan, J., Shinn, C., Xu, K., Cui, J., Klimiashvili, G., Xiao, G., Zheng, P., Li, B., Zhou, Y., Ye, Z., You, W., Zheng, T., Brown, D., Wang, P., Cai, R., Demouth, J., Owens, J. D., Hu, X., Han, S., Liu, T., and Mao, H. Blassst: Dynamic blocked attention sparsity via softmax thresholding, 2025. URL <https://arxiv.org/abs/2512.12087>.

Zhang, J., Wei, J., Huang, H., Zhang, P., Zhu, J., and Chen, J. SageAttention: Accurate 8-bit attention for plug-and-play inference acceleration, 2025. URL <https://arxiv.org/abs/2410.02367>.

A. Implementation of 8-bit Operations

A.1. HiF8 Implementation

To simplify the implementation of the experiments, this paper consistently uses HiF8 (Luo et al., 2024) as the unified 8-bit number format. As indicated in (Luo et al., 2024), HiF8 can harness the advantage of E4M3 and E5M2 with a wider dynamic range for a best-of-both-worlds representation. With no prior knowledge of the dynamic ranges of scores in the model and their exponents, HiF8 is expected to be much more robust compared to other FP8 formats. As no hardware implementation of powers of two in 8-bit numbers is currently available, the utilization of HiF8 operations is implemented in a simulated manner by taking advantage of FP16 operations. All of the inputs are truncated to HiF8 and then retained back to FP16 for following steps, as shown in line 2 and 3 in Algorithm 2. Then the required operations, e.g., powers of 2, are performed in FP16. Finally, the numbers are converted to HiF8 to truncate the extra bits provided by FP16. This procedure is summarized in Algorithm 2.

Algorithm 2 Simulation of Powers of Two in HiF8.

- 1: **Input:** data x_{FP16} in FP16.
- 2: Convert x_{FP16} to HiF8 x_{HiF8} .
- 3: Convert x_{HiF8} to FP16 \hat{x}_{FP16} .
- 4: Compute powers of two $y_{\text{FP16}} = \exp2(\hat{x}_{\text{HiF8}})$
- 5: Convert y_{FP16} to HiF8 y_{HiF8} .
- 6: Convert y_{HiF8} to FP16 \hat{y}_{FP16} .
- 7: **Return:** \hat{y}_{FP16} .

B. Ablation Experiments Results

B.1. The Language Models

Table 5 and 6 show the scores of Qwen3 and Llama-3.1 scores on different sub-tasks in MMLU-Pro benchmark suite, respectively. All of the accuracies that showing a degradation more than 1% (at least two-sample differences) of the task have been highlighted in red.

Task \ Setup	Default	Exp2 HiF8	E2E HiF8
Task			
Computer Science	78.29	76.34	77.32
Math	85.79	85.34	84.97
Chemistry	76.86	76.94	76.24
Engineering	54.39	51.70	51.60
Law	49.59	49.23	49.59
Biology	87.31	86.33	86.75
Health	74.57	74.69	74.08
Physics	78.37	78.44	77.75
Business	76.93	77.69	76.17
Philosophy	69.94	66.93	68.34
Economics	82.35	81.28	81.64
Other	70.35	70.78	70.35
Psychology	78.20	77.69	77.32
History	66.14	63.78	63.25
Overall	73.59	72.96	72.53

Table 5. Accuracy of Qwen3-30B-A3B on different tasks in MMLU-Pro with different setups. The accuracy is calculated in percentage and higher values are preferable.

Task \ Setup	Default	Exp2 HiF8	E2E HiF8
Computer Science	48.54	45.85	48.78
Math	47.30	49.15	48.85
Chemistry	40.46	37.72	37.46
Engineering	25.39	23.84	23.32
Law	32.43	31.06	31.34
Biology	64.16	66.67	66.11
Health	56.11	55.62	56.60
Physics	39.65	39.26	39.18
Business	51.71	50.95	49.68
Philosophy	54.27	43.29	42.69
Economics	49.68	55.57	53.67
Other	49.68	49.35	46.75
Psychology	61.15	60.03	61.15
History	43.04	41.73	41.47
Overall	46.01	45.51	45.19

Table 6. Accuracy of Llama-3.1-8B on different tasks in MMLU-Pro with different setups. The accuracy is calculated in percentage and higher values are preferable.

Table 7 and 8 show the scores of Qwen3 and Llama-3.1 scores on different difficulty levels in MATH500.

Level \ Setup	Default	Exp2 HiF8	E2E HiF8
1	97.67	97.67	95.35
2	92.22	93.33	96.67
3	86.67	90.48	87.62
4	75.78	77.34	75.78
5	58.96	59.70	61.19
Overall	78.4	80.0	79.8

Table 7. Accuracy of Qwen3-30B-A3B on different difficulty levels in MATH500 with different setups. The accuracy is calculated in percentage and higher values are preferable.

B.2. The Multi-modal Models

Figure 5-12 show the generated videos from different setups. It extracts 4 frames from the generated videos for reference.

Level \ Setup	Default	Exp2 HiF8	E2E HiF8
1	83.72	86.05	93.02
2	68.89	71.11	64.44
3	53.33	58.10	57.14
4	42.19	34.38	42.19
5	19.40	19.40	19.40
Overall	46.8	46.4	47.6

Table 8. Scores of Llama-3.1-8B on different difficulty levels in MATH500 with different setups. The accuracy is calculated in percentage and higher values are preferable.

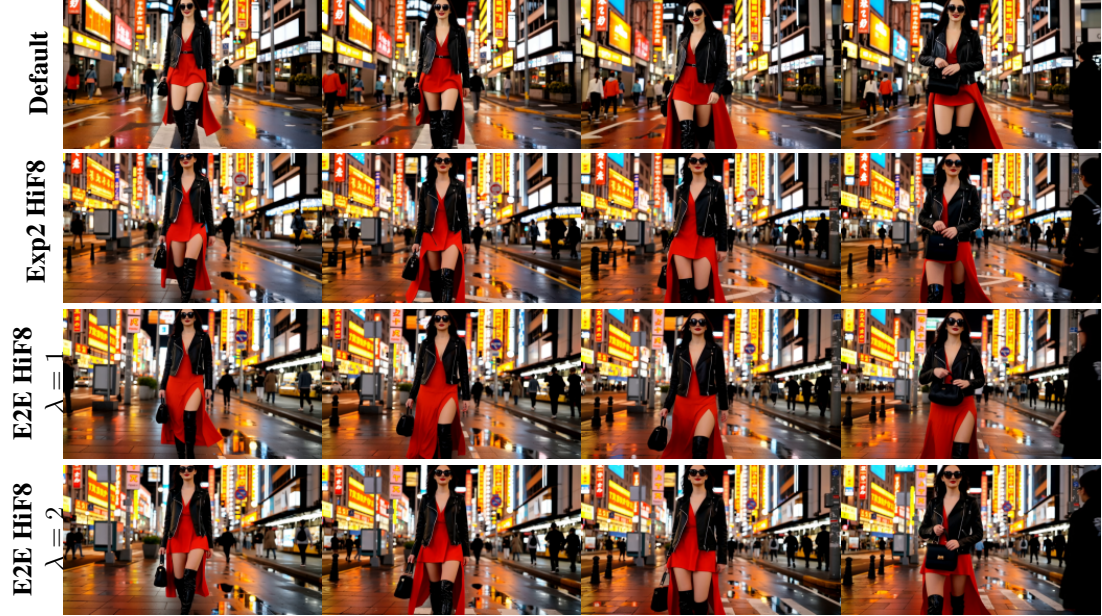


Figure 5. Prompt 1: “A stylish woman walks down a Tokyo street filled with warm glowing neon and animated city signage. She wears a black leather jacket, a long red dress, and black boots, and carries a black purse. She wears sunglasses and red lipstick. She walks confidently and casually. The street is damp and reflective, creating a mirror effect of the colorful lights. Many pedestrians walk about.”



Figure 6. Prompt 2: “Several giant wooly mammoths approach treading through a snowy meadow, their long wooly fur lightly blows in the wind as they walk, snow covered trees and dramatic snow capped mountains in the distance, mid afternoon light with wispy clouds and a sun high in the distance creates a warm glow, the low camera view is stunning capturing the large furry mammal with beautiful photography, depth of field.”



Figure 7. Prompt 3: “A movie trailer featuring the adventures of the 30 year old space man wearing a red wool knitted motorcycle helmet, blue sky, salt desert, cinematic style, shot on 35mm film, vivid colors.”

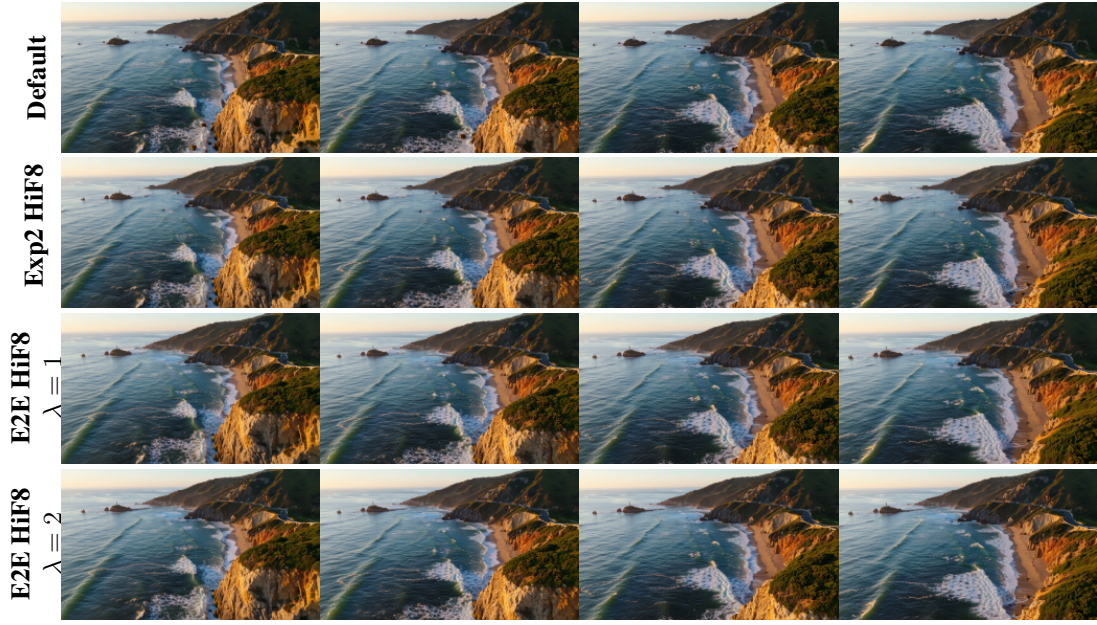


Figure 8. Prompt 4 “Drone view of waves crashing against the rugged cliffs along Big Sur’s gray point beach. The crashing blue waters create white-tipped waves, while the golden light of the setting sun illuminates the rocky shore. A small island with a lighthouse sits in the distance, and green shrubbery covers the cliff’s edge. The steep drop from the road down to the beach is a dramatic feat, with the cliff’s edges jutting out over the sea. This is a view that captures the raw beauty of the coast and the rugged landscape of the Pacific Coast Highway.”



Figure 9. Prompt 5: “Animated scene features a close-up of a short fluffy monster kneeling beside a melting red candle. The art style is 3D and realistic, with a focus on lighting and texture. The mood of the painting is one of wonder and curiosity, as the monster gazes at the flame with wide eyes and open mouth. Its pose and expression convey a sense of innocence and playfulness, as if it is exploring the world around it for the first time. The use of warm colors and dramatic lighting further enhances the cozy atmosphere of the image.”



Figure 10. Prompt 6: “A gorgeously rendered papercraft world of a coral reef, rife with colorful fish and sea creatures.”

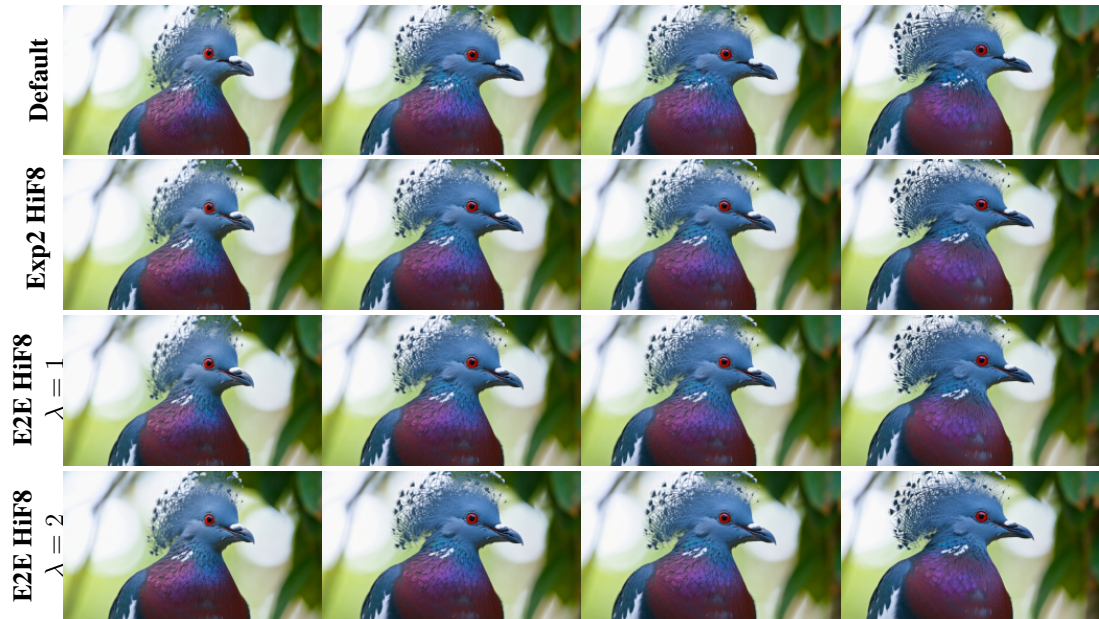


Figure 11. Prompt 7: “This close-up shot of a Victoria crowned pigeon showcases its striking blue plumage and red chest. Its crest is made of delicate, lacy feathers, while its eye is a striking red color. The bird’s head is tilted slightly to the side, giving the impression of it looking regal and majestic. The background is blurred, drawing attention to the bird’s striking appearance.”



Figure 12. Prompt 8: “Photorealistic closeup video of two pirate ships battling each other as they sail inside a cup of coffee.”